Low-Order Modeling of Vehicle Roll Dynamics

Bridget C. Hamblin, Ryan D. Martini, John T. Cameron, and Sean N. Brennan, *Member, IEEE*

***Abstract*— This work presents results of an ongoing investigation into models and control strategies suitable to prevent vehicle rollover due to untripped driving maneuvers. For use as a design model for controller synthesis, low-order models are sought that have sufficient complexity to characterize a vehicle's roll behavior, yet are not unnecessarily complex or nonlinear. To compare different low-order models found in literature, this work investigates the validity of several roll dynamic models by comparing model prediction to experiment in both the time and frequency domains. Discussion is also given on methods for parametric fitting of the models and areas where significant model error is observed.**

***Index Terms*—Vehicle rollover, vehicle dynamics, modeling of dynamic systems**

I. Introduction

Accidental death due to motor vehicle accidents claim over 1.2 million life-years of unlived life each year, and is the largest premature death factor for those under the age of 65 [1]. Vehicle accidents are the single largest cause of fatalities for males 44 years and under and for females 34 years and under [2]. These deaths are sudden, and often strike when a person is at the peak of both their professional and personal/family life.

Among the myriad causes of vehicle accidents, rollover stands out as an area deserving of particular focus. While vehicle rollover is involved in only 2.5% of the 11 million accidents a year, it accounts for approximately 20% of all fatalities [3].

To study rollover, the National Highway Traffic Safety Administration (NHTSA) has developed a number of transient maneuvers that are observed to induce untripped wheel lift or even untripped vehicle rollover in some vehicle models [4, 5]. While this experimental approach is unarguably valid for illustrating shortcomings in vehicle behavior, the method does have shortcomings. In particular, it is difficult to definitively establish from only a very small subset of tests whether or not roll safety is ensured over all possible transient maneuvers. Additionally, experimental results do not directly translate into a vehicle model suitable for rollover mitigation through feedback control. Both factors highly motivate the development of vehicle roll models.

In considering the choice of which roll dynamic model to use, the choice of complexity in the model should match well with the intended use of the model. This study is focused on finding dynamic models that are well suited to the design and implementation of online, real-time controllers to prevent the onset of rollover. A goal of this work and particular departure from previous studies is to not only understand and validate the linear vehicle dynamics of roll behavior, but also to understand the relative impact of various assumptions in creating the vehicle models to ensure the use of the simplest model possible in later controller synthesis.

The remainder of the paper is organized as follows: Section 2 presents preliminaries on nomenclature and model formulation. Section 3 presents several models that will be compared in this study. Section 4 discusses how the inertial parameters of the models were obtained. Section 5 discusses experimental fitting of linear tire parameters. Section 6 details modifications to the linear tire to account for camber. Section 7 presents dynamic model fits. Conclusions summarize the main points.

II. Preliminaries

The following notation is used for each of the models described in this work:

U	Longitudinal velocity (body-fixed frame)
m, m_s	Vehicle mass and sprung mass respectively
I_{xx}, I_{yy}, I_{zz}	Inertia about roll (X), pitch (Y),vertical (Z) axis
I_{xz}	Inertia product
l_f, l_r	Front- and Rear-axle-to-CG distances
L	Track of vehicle ($l_f + l_r$)
K_φ	Effective roll stiffness of the suspension
D_φ	Effective roll damping of the suspension
h	height from roll axis to CG
α_f , α_r	Slip angle of the front, rear tires
β	Slip angle of the vehicle body
C_f, C_r	Front, Rear cornering stiffness
δ_f	Front steering angle

For ease of comparison model to model, each of the models is presented in a compact symbolic notation of the form:

B. Hamblin and R. Martini are current graduate students at Penn State.

J. T. Cameron is a recent graduate from Mechanical and Nuclear Engineering who is now working with Harris Corp. in Florida.

S. Brennan is an Assistant Professor in the Mechanical & Nuclear Engineering Department, Penn State University, 318 Leonhard Building, University Park, PA 16802. He shares a joint appointment with the Pennsylvania Transportation Institute. (corresponding author, phone (814)863-2430; sbrennan@psu.edu)

$$M \cdot \ddot{q} + D \cdot \dot{q} + K \cdot q = F \cdot u_f \quad (1)$$

where i denotes the model number (1 to 4 for this study), and

$$q = \{y \quad \psi \quad \phi\}^T \quad (2)$$

which denotes the lateral position, yaw angle, and roll angle respectively. The input to the model,

$$u = \{F_f \quad F_r\}^T \quad (3)$$

denotes the front and rear lateral tire forces respectively. The general MDK form described by Eq. (1) allows for an intuitive term-by-term comparison between different models. Further, this MDK form can be readily transformed to the general state-space form of:

$$\frac{dx}{dt} = A \cdot x + B \cdot u \quad (4)$$

with the state vector,

$$x = \lfloor V \quad r \quad \phi \quad \dot{\phi} \rfloor \quad (5)$$

representing lateral velocity, yaw rate, roll angle and roll rate respectively. The transformation from MDK form to state space is given by the following. Let:

$$R = \begin{bmatrix} 1 & 0 & 0 \\ 0 & 1 & 0 \\ 0 & 0 & 0 \\ 0 & 0 & 1 \end{bmatrix}, \quad S = \begin{bmatrix} 0 & 0 & 0 \\ 0 & 0 & 0 \\ 0 & 0 & 1 \\ 0 & 0 & 0 \end{bmatrix}, T = \begin{bmatrix} 0 & 0 & 0 & 0 \\ 0 & 0 & 0 & 0 \\ 0 & 0 & 0 & 1 \\ 0 & 0 & 0 & 0 \end{bmatrix} \quad (6)$$

and define,

$$E = R \cdot (M - I_3) \cdot R^T + I_4 \quad (7)$$

where I_n represents the identity matrix of size n. Then the state-space matrices A and B are obtained from matrices M, D, K and F as:

$$A = E^{-1} \cdot (-R \cdot D \cdot R^T - R \cdot K \cdot S^T + T)$$
$$B = E^{-1} \cdot (R \cdot F) \quad (8)$$

The state-space form more conveniently allows numerical simulation and model comparisons used in later sections.

III. Vehicle Models

A search of recent literature found over two dozen unique vehicle models inclusive of roll dynamics, but of these, only a few are chosen for further analysis. Considerations used to eliminate certain models are detailed in previous work (see [6]), but the main criteria are based primarily on model complexity, whether or not the model had been validated experimentally by the authors of the model, and how easily model parameters can be measured or inferred.

To emphasize the similarity between the models used in this study, each is presented in the same coordinate system regardless of the coordinate system used in the original publication of the model [7-9]. Herein they all follow the SAE right-handed sign convention shown in Fig 1.

For brevity, details of each model derivation have been omitted from this work, but further details can be found in the original publications [7-9] and in previous work [6]. A discussion of the notable similarities and differences between the different models can be found in [6].

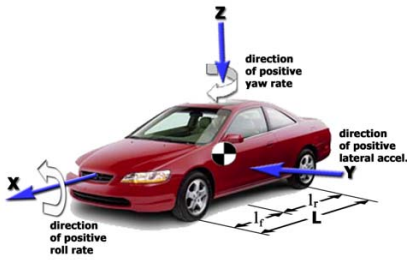

Figure 1: SAE Coordinate System

A. Model 1 - 3DOF Model Assuming Existence of Sprung Mass and No X-Z Planar Symmetry

The most complex model considered in this work is derived by assuming a sprung and unsprung mass, and assuming the unsprung mass has a non-symmetric mass distribution about the x-z plane. It is motivated by the model presented by Mammar et. al. [10]; further details and assumptions are listed therein. Following the MDK form specified earlier, the MDK matrices are given by:

$$M_1 = \begin{bmatrix} m & 0 & m_s h \\ 0 & I_{zz} & -I_{xz} \\ m_s h & -I_{xz} & I_{xx} + m_s h^2 \end{bmatrix} \quad (9)$$

$$D_1 = \begin{bmatrix} 0 & mU & 0 \\ 0 & 0 & 0 \\ 0 & m_s h U & D_\phi \end{bmatrix} \quad (10)$$

$$K_1 = \begin{bmatrix} 0 & 0 & 0 \\ 0 & 0 & 0 \\ 0 & 0 & K_\phi - m_s g h \end{bmatrix} \quad (11)$$

$$F_1 = \begin{bmatrix} 1 & 1 \\ a & -b \\ 0 & 0 \end{bmatrix} \quad (12)$$

B. Model 2 - 3DOF Model Assuming Existence of Sprung Mass and X-Z Planar Symmetry

A common assumption in the above model is that the vehicle is symmetric about the x-z plane, thus making I_{xz} zero and eliminating all cross terms. An example of this is presented by Kim and Park in [8]. In presenting this model, some authors absorb the suspended mass term, *mgh*, in the (3, 3) element of the K matrix, into the roll stiffness. For example, Kim and Park cited above make this assumption. Placing the equations of motion into the form specified by Eq. (1), the damping, stiffness, and force matrices remain the same,

$$D_2 = D_1, K_2 = K_1, F_2 = F_1 \quad (13)$$

while the mass matrix becomes:

$$M_2 = \begin{bmatrix} m & 0 & m_s h \\ 0 & I_{zz} & 0 \\ m_s h & 0 & I_{xx} + m_s h^2 \end{bmatrix} \quad (14)$$

With the assumption of a symmetric mass distribution, the yaw dynamics are not directly coupled to the roll and sideslip dynamics in the MDK form. In state-space, they can only be coupled through the inversion of the mass matrix, E^{-1}, and through the tire forces, if these forces are dependent on roll.

C. Model 3 - 3DOF Model Assuming Sprung Mass Only

In addition to the assumptions given previously, it is sometimes assumed that the entire mass of the vehicle is concentrated at the sprung mass. The paper by Carlson et. al [7] uses this assumption. To modify previous models to express this assumption, the unsprung mass is made zero and the sprung mass is made equal to the total mass of the vehicle. The resulting MDK matrices are:

$$M_3 = \begin{bmatrix} m_s & 0 & m_s h \\ 0 & I_{zz} & 0 \\ m_s h & 0 & I_{xx} + m_s h^2 \end{bmatrix} \quad (15)$$

$$D_3 = \begin{bmatrix} 0 & m_s U & 0 \\ 0 & 0 & 0 \\ 0 & m_s h U & D_\phi \end{bmatrix} \quad (16)$$

The F and K matrices are unchanged, e.g.

$$K_3 = K_2,\ F_3 = F_2 \quad (17)$$

D. Model 4- 2DOF Model Assuming No Roll Dynamics

Finally, if one assumes that the sprung mass height is zero, the roll dynamics are completely eliminated because there is no longer any coupling from yaw or lateral velocity into roll. Without this coupling, there is no energy input to the roll model other than initial conditions. This assumption produces the well-known "bicycle model" which describes the vehicle's planar dynamics [11].

$$M_4 = \begin{bmatrix} m & 0 & 0 \\ 0 & I_{zz} & 0 \\ 0 & 0 & 0 \end{bmatrix} \quad (18)$$

$$D_4 = \begin{bmatrix} 0 & mU & 0 \\ 0 & 0 & 0 \\ 0 & 0 & 0 \end{bmatrix} \quad (19)$$

$$K_4 = \begin{bmatrix} 0 & 0 & 0 \\ 0 & 0 & 0 \\ 0 & 0 & 0 \end{bmatrix} \quad (20)$$

Again, the F matrix is unchanged:

$$F_4 = F_3 \quad (21)$$

While this model does not include any roll dynamics and only exhibits lateral and yaw dynamics, it is included in this work because bicycle model parameters are used in all other models. It is therefore important to consider this model in order to find or fit chassis parameters for models 1-3.

IV. Obtaining Vehicle Inertial Parameters

To analyze validity of the models to describe vehicle chassis behavior, experiments were performed on a 5-door 1992 Mercury Tracer station wagon available at Penn State's Pennsylvania Transportation Institute test track. A significant improvement over previous work is that this study was conducted using Novatel's GPS/INS "SPAN" system. This GPS/INS system is based off two Novatel OEM4 dual frequency GPS receivers and the Honeywell HG1700 military tactical-grade IMU. This combination can provide estimates of position, velocity and attitude at rates up to 100Hz. In differential carrier phase fixed-integer mode and with continuous presence of GPS data, the system achieves a position solution with an accuracy of 2 cm. Attitude can be estimated with a 1-sigma accuracy of 0.013 degrees for roll, 0.04 deg for pitch and 0.04 degrees for yaw. All velocity errors are 0.007 m/s (one sigma) [12].

Many of the inertial parameters appearing in models 1-4 are easily measured or obtained from the National Highway Traffic Safety Administration database [13]. The table below presents these parameter values, units, and their source.

Table 1: Inertial parameter values

Variable	Value	Units	How obtained
m	1030	kg	Measured
m_s	824	kg	Estimated
W_f	6339	N	Measured
W_r	3781	N	Measured
l_f	0.93	m	NHTSA*
l_r	1.56	m	NHTSA*
L	2.49	m	Calculated
h	0.25	m	Measured
I_{zz}	1850	kg-m^2	NHTSA*
I_{yy}	1705	kg-m^2	NHTSA
I_{xx}	375	kg-m^2	NHTSA
I_{xz}	72	kg-m^2	NHTSA

*measurements were also made and these confirmed the NHTSA value to within a few percent

Estimates of sprung mass, m_s, were obtained by approximating the sprung mass as 0.8 times the total mass. The CG height was found to be 0.25 meters above the roll axis. The roll axis was found by video-taping the vehicle undergoing a rocking motion from the front and rear, determining the center of rotation at the front and rear axles, then using similar triangles to determine the axis of rotation at the center-of-gravity of the vehicle. Note that the sprung-mass height above the roll-axis is not the height of the CG above the road surface reported by NHTSA, 0.52 meters for this vehicle.

V. Fitting Bicycle Model Tire Parameters

Several model parameters, especially the tire cornering stiffnesses, require experimental fitting and careful consideration of the tire's impact on the model behavior. The models presented in this study lump right- and left-side

lateral tire forces to a single force on the front and rear axles, F_f and F_r. This single-wheel representation of a two-wheel axle is why the bicycle model is so named. Further, it is assumed that the lateral forces acting on each tire are directly proportional to the tire slip with proportionality constants on the front and rear tires of C_f and C_r respectively:

$$F_f = C_f \alpha_f, F_r = C_r \alpha_r, \quad (22)$$

The slip angles, α_i, are defined as the angle between the tire's orientation and the velocity vector of the center of the tire:

$$\alpha_f = \tan^{-1}\left(\frac{V + l_f \cdot r}{U}\right) - \delta_f \approx \frac{V + l_f \cdot r}{U} - \delta_f \quad (23)$$

$$\alpha_f = \tan^{-1}\left(\frac{V - l_r \cdot r}{U}\right) \approx \frac{V - l_r \cdot r}{U} \quad (24)$$

The simplifying assumptions made for Eqs. (23) and (24) are that the slip angles are small enough to allow a linear approximation and that right- and left-side differences in tire forces are negligible. With these assumptions, the tire forces can be written as:

$$F_f = C_f\left(\frac{V + l_f \cdot r}{U} - \delta_f\right) \quad (25)$$

$$F_r = C_r\left(\frac{V - l_r \cdot r}{U}\right) \quad (26)$$

Longitudinal forces acting upon the tires are assumed to be zero, and longitudinal velocity, *U*, is assumed to be constant.

The resulting expressions, when substituted into models 1-4 above, predict linear models. However, it is well known that the linearity assumption is violated under aggressive maneuvering. Others have noted that if the lateral acceleration remains below 0.4 g's, then assumptions of linearity appear to hold (many cite [14] as support). Therefore, care was taken in all testing to ensure that the experiments were conducted at lower accelerations.

To test whether or not linearity is actually preserved in the measured data, two frequency responses were conducted on the vehicle: one for steering inputs of small amplitude (1/4 rotation of the hand wheel) and one for large amplitudes (slightly less than 1/2 rotation of the handwheel). The resulting Bode plots are overlaid and shown in Figs. 1 and 2 below for the two states of the bicycle model, yaw rate and lateral velocity recorded at a speed of 25 mph. The linearity of the models is evident.

To find the cornering stiffnesses, two methods were used that are both based on steady-state data. Steady-state data was chosen since these data should be least influenced by model-to-model differences in high-order dynamics. The first fitting method attempts to match the DC gains of the sinusoidal frequency responses of Figs. 1 and 2. The second method is based on matching measured responses from steady-state turning around a skid-pad circle. Each is detailed below.

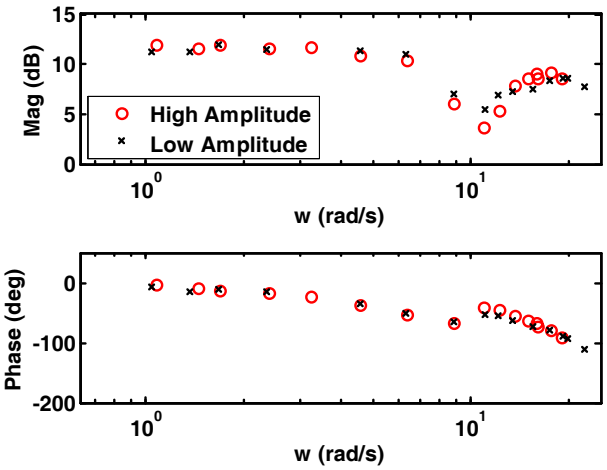

Figure 1: Frequency Response, Steering Input to Lateral Velocity

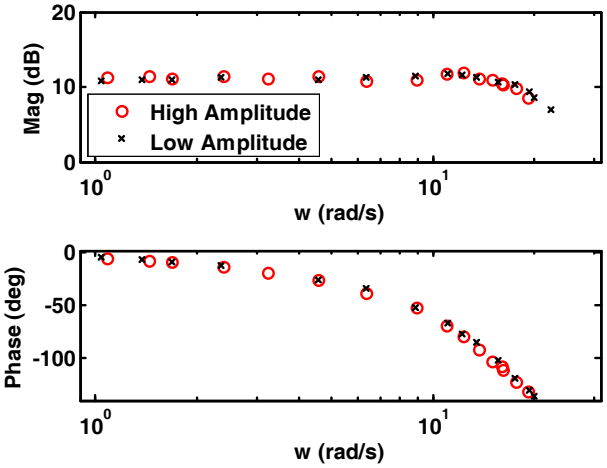

Figure 2: Frequency Response, Steering Input to Yaw Rate,

From the state-space form of Eq. (4), the DC gains, G, of the bicycle model from steering input to state output are given by:

$$G = D - CA^{-1}B \quad (28)$$

For lateral velocity, *V*, this DC gain was parametrically solved to be:

$$G_V = \frac{U \cdot \left((C_f C_r) \cdot l_r \cdot L + C_f (l_f \cdot m \cdot U^2)\right)}{C_f C_r \cdot (l_r^2 + l_f^2 + 2 \cdot l_f \cdot l_r) + m \cdot U^2 (C_f l_f - C_r \cdot l_r)} \quad (29)$$

and for yaw rate, *r*:

$$G_r = \frac{U \cdot (C_f C_r) \cdot L}{C_f C_r \cdot (l_r^2 + l_f^2 + 2 \cdot l_f \cdot l_r) + m \cdot U^2 (C_f \cdot l_f - C_r \cdot l_r)} \quad (30)$$

The numerical values of G_V and G_r can be read from Figs. 1 and 2 as 3.804 m/s lateral velocity per radian of steering input and 3.599 rad/sec yaw rate per radian of steering input,

respectively. Rearranging the above equations, one can directly solve for cornering stiffnesses after substitution of known vehicle parameters:

$$C_r = \frac{(l_f \cdot m \cdot U^2 \cdot G_r)}{(G_v - l_r \cdot G_r) \cdot L} = \text{-88,385} \frac{\text{N}}{\text{rad}} \qquad (31)$$

$$C_f = \frac{(-U^2 \cdot m \cdot G_r \cdot C_r \cdot l_r)}{(C_r \cdot U \cdot L - G_r \cdot C_r \cdot L^2 - U^2 \cdot m \cdot G_r \cdot l_f)} = \text{-83,014} \frac{\text{N}}{\text{rad}}$$

These values, when substituted into the bicycle model, did appear to match the measured sinewave time responses obtained in conducting the frequency responses. Additionally, it appeared to match maneuvers that did not excite significant roll, e.g. lane changes and the like. However, the model had a very poor fit for vehicle response data collected during steady-state turning on the skid pad. In an attempt to reconcile steady-turning data, a method was sought to determine cornering stiffness values for this data alone.

For steady-state turning around a constant radius circle, the side-slip, $\beta = V/U$, measured at the center-of-gravity of the vehicle is given by [15]:

$$\beta = \frac{l_r}{R} + \frac{W_r}{C_r \cdot g} \frac{U^2}{R} \qquad (32)$$

The side-slip is clearly dependent on speed and radius of the turning circle. This therefore suggests a method to determine the rear cornering stiffness: measure side slip on the vehicle and slowly increase the vehicle speed traversing a steady circle to the point where side slip becomes zero. At $\beta = 0$, the above expression gives the cornering stiffness as:

$$C_r = -\frac{W_r}{l_r \cdot g} U^2 \qquad (33)$$

Note that this expression is independent of the radius of the turn. Fig. 3 below shows data collected during one of many maneuvers to determine the speed at which zero sideslip occurred. Repeated measurements showed that zero sideslip occurred for this vehicle around 14.1 m/s. Using values measured for the vehicle, the calculated rear cornering stiffness was found to be $C_r = -49{,}300 N/rad$.

The front cornering stiffness can be found using the relationship at steady state between steering input and front and rear cornering stiffness:

$$\delta = \frac{L}{R} + \left(\underbrace{\frac{W_r}{C_r} - \frac{W_f}{C_f}}_{Kus} \right) \frac{U^2}{g \cdot R} \qquad (34)$$

where $K_{us} = \left(\frac{W_r}{C_r} - \frac{W_f}{C_f} \right)$ is the understeer gradient (assuming negative cornering stiffnesses). So

$$C_f = \frac{-W_f}{\left(\delta_f - \frac{L}{R} \right) \frac{g \cdot R}{U^2} + \frac{W_r}{C_r}} \qquad (35)$$

For the sideslip maneuvers as shown in Fig. 3, the average steering input, δ_f, during the point at which sideslip passed through zero were approximately 0.0830 rad of front wheel angle. This gives an approximate value of $C_f = -57{,}700\ N/rad$.

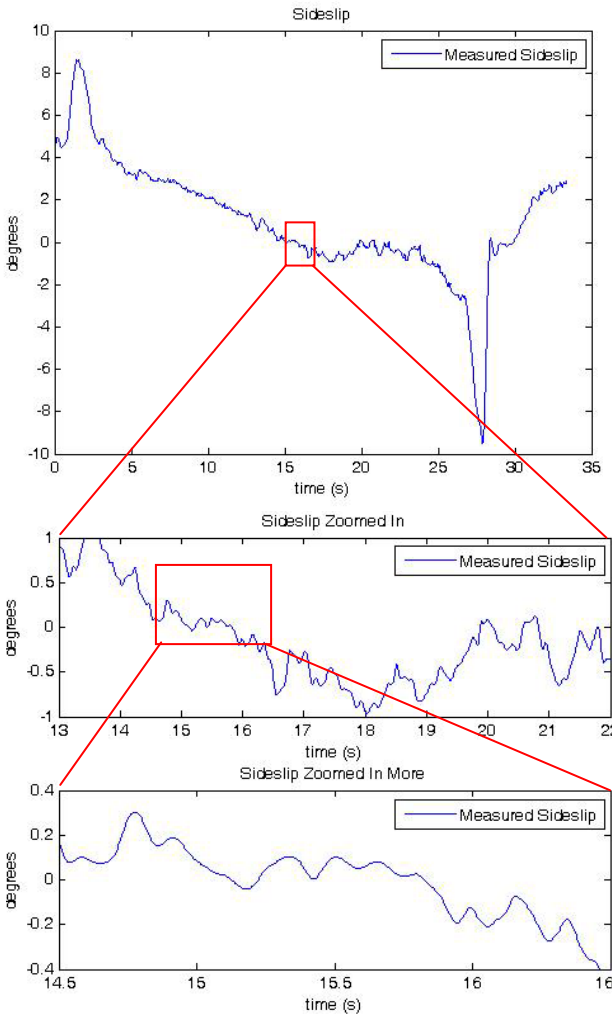

Figure 3: Using the zero-sideslip condition to measure cornering stiffness

The understeer gradient can also be used to find the front cornering stiffness from Eq. (34):

$$C_f = \frac{W_f \cdot C_r}{W_r - C_r \cdot K_{us}} \qquad (36)$$

Measurements of the understeer gradient can be obtained by plotting steering input versus lateral acceleration as shown in Fig. 4 below. Using these results, an understeer gradient was found to be $K_{us} = 0.016$. This gives a front cornering stiffness value of $C_f = -68{,}400\ N/rad$ which is roughly 15% different from the previous value.

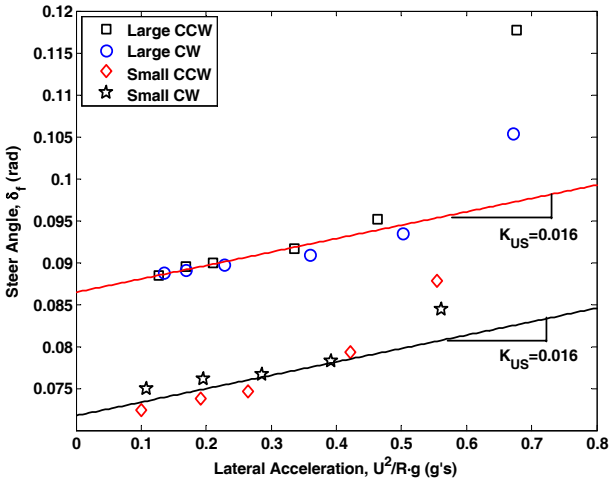

Figure 4: Steady state steering measurements measured as a function of lateral acceleration for two different radii turning circles along two different directions, clockwise and counter-clockwise.

When comparing the cornering stiffness values obtained from the steady-state circle methods to the steady-state circle time responses, the agreement was good. However, the same cornering stiffness values poorly matched the frequency response data. With these observations, it was inferred that another mechanism to produce tire force was occurring only during steady turning. Therefore, the model for tire force generation was revisited.

VI. Tire Models with Camber

The previous analysis suggests that there is a significant tire force generation mechanism that is dependent on whether or not the vehicle is in a steady turn. One possible explanation for this behavior is that the tire model is dependent on the vehicle's roll angle, an inference supported by the work of others. For example, in the reference [8], Kim and Park introduce a incremental change in force on the tire model in the form of $\frac{\partial \alpha_f}{\partial \phi}\phi$. This effect is commonly known as "roll steer" and is usually assumed to be a constant value when the amount of tire slip is small. According to [8], the magnitude of the coefficient for the front tires was 0.2, and -0.2 for the rear tires.

To find the roll-steer parameters for this study, it appears that one must simultaneously solve for four parameters – two cornering stiffnesses and two camber coefficients – to match the measured steady-state data. However, here it is assumed that the cornering stiffnesses obtained by matching the frequency responses are not greatly influenced by tire camber due to the very low roll angles exhibited at low frequencies. Therefore, one only needs to consider the turning circle data to measure the influence of tire camber.

To experimentally obtain parameters representative of tire camber, the following procedure is utilized. First, the tire forces are assumed to depend on roll by the following relationship:

$$\begin{aligned} F_f &= C_f \alpha_f + C_{\phi f}\phi_{wf} \\ F_r &= C_r \alpha_r + C_{\phi r}\phi_{wr} \end{aligned} \tag{37}$$

where ϕ_{wf} and ϕ_{wr} are the camber angles of the front and rear tires, and $C_{\phi f}$ and $C_{\phi r}$ are the proportionality constants representing the change in tire force as a function of roll angle, $C_{\phi f} = \frac{\partial F_f}{\partial \phi}$, etc. Now define the change in wheel camber angle as a function of the entire vehicle's roll angle via a proportionality constant, *S*:

$$\begin{aligned} \phi_{wf} &= S_f \cdot \phi_v \\ \phi_{wr} &= S_r \cdot \phi_v \end{aligned} \tag{38}$$

The steady-state roll angle of the vehicle for a constant velocity, constant radius turn, ϕ_v, is solved by moment balance:

$$\phi_v = \frac{h}{K_\phi} \cdot \frac{m_s U^2}{R} \tag{39}$$

A steady-state force balance for a vehicle traversing a steady-state turn gives the following slip angles:

$$\begin{aligned} \alpha_f &= \frac{1}{C_{\alpha f}}\left[\frac{l_r}{L}\cdot\frac{mU^2}{R} - \frac{C_{\phi f}\cdot m_s \cdot h}{k_r} S_f \frac{U^2}{R}\right] \\ \alpha_r &= \frac{1}{C_{\alpha r}}\left[\frac{l_f}{L}\cdot\frac{mU^2}{R} - \frac{C_{\phi r}\cdot m_s \cdot h}{k_r} S_r \frac{U^2}{R}\right] \end{aligned} \tag{40}$$

which can be more compactly represented as:

$$\begin{aligned} \alpha_f &= \frac{1}{S_f}\left[\frac{l_r}{L}\cdot\frac{mU^2}{R} - C_f^* \frac{U^2}{R}\right] \\ \alpha_r &= \frac{1}{S_r}\left[\frac{l_f}{L}\cdot\frac{mU^2}{R} - C_r^* \frac{U^2}{R}\right] \end{aligned} \tag{41}$$

with

$$\begin{aligned} C_f^* &= \frac{C_{\phi f} m_s h}{k_s} S_f \\ C_r^* &= \frac{C_{\phi r} m_s h}{k_s} S_r \end{aligned} \tag{42}$$

The steady-state steering input necessary to traverse a constant radius turn at constant speed is therefore given by:

$$\delta_f = \frac{L}{R} - \frac{1}{C_f}\left[\frac{l_r}{L}\cdot\frac{mU^2}{R} - C_f^*\frac{U^2}{R}\right] + \frac{1}{C_r}\left[\frac{l_f}{L}\cdot\frac{mU^2}{R} - C_r^*\frac{U^2}{R}\right] \tag{43}$$

which allows one to solve for the steady-state steering gains for a constant velocity, constant radius turn.

$$\left.\frac{r}{\delta_f}\right|_{circle} = \frac{\frac{U}{R}}{\frac{L}{R} - \frac{1}{C_f}\left[\frac{l_r}{L}\cdot\frac{mU^2}{R} - C_f^*\frac{U^2}{R}\right] + \frac{1}{C_r}\left[\frac{l_f}{L}\cdot\frac{mU^2}{R} - C_r^*\frac{U^2}{R}\right]} \tag{44}$$

and

$$\left.\frac{V}{\delta_f}\right|_{circle} = \frac{U\cdot\left(\frac{l_r}{R}+\alpha_r\right)}{\frac{L}{R}-\frac{1}{C_f}\left[\frac{l_r}{L}\cdot\frac{mU^2}{R}-C_f^*\frac{U^2}{R}\right]+\frac{1}{C_r}\left[\frac{l_f}{L}\cdot\frac{mU^2}{R}-C_r^*\frac{U^2}{R}\right]} \quad (45)$$

The steady-state values of these two transfer functions are easily obtained using the turning data. This allows the values of C_f^* and C_r^* to be directly calculated since all other parameters are known.

VII. Dynamic Model Fitting

In previous work [6], examination of the phase lag observed in the frequency response data showed that a model of tire lag was necessary to obtain a reasonable model fit. The tire-lag phenomenon is commonly modeled as a first-order system with zero steady-state gain [16]. In previous work [6], a first-order tire lag model was introduced on the front steering input. After consultation with the authors of [7] and reviewing [11, 17], the following model of tire lag was used which considers tire lag as a function of tire slip on the front and rear tires:

$$\frac{dF_f}{dt} = \frac{U}{\sigma}\left(C_f\left(\frac{V+l_f\cdot r}{U}-\delta_f\right)-F_f\right) \quad (46)$$
$$\frac{dF_r}{dt} = \frac{U}{\sigma}\left(C_r\left(\frac{V-l_r\cdot r}{U}\right)-F_r\right)$$

The best fits were obtained with a tire lag value of sigma = 0.8 for front and 0.6 for rear, but difference between these and an average value of 0.7 were minor. The above tire-lag model is used hereafter for all tire force calculations.

A. Frequency Response Tests – Roll Model Fit

The two parameters that remained to be estimated for roll model fitting were K_φ and D_φ. To accomplish this, these parameters were varied manually until the models best matched the frequency response data. The resulting frequency-domain fits are seen in Figs. 5-7, where both experimental data and model are shown. The data was collected at 25 mph.

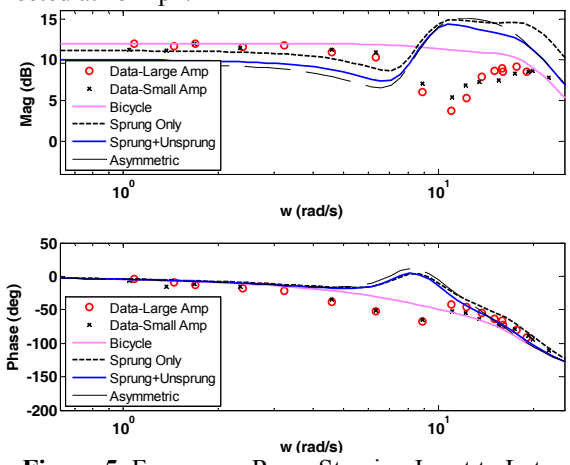

Figure 5: Frequency Resp. Steering Input to Lateral Velocity

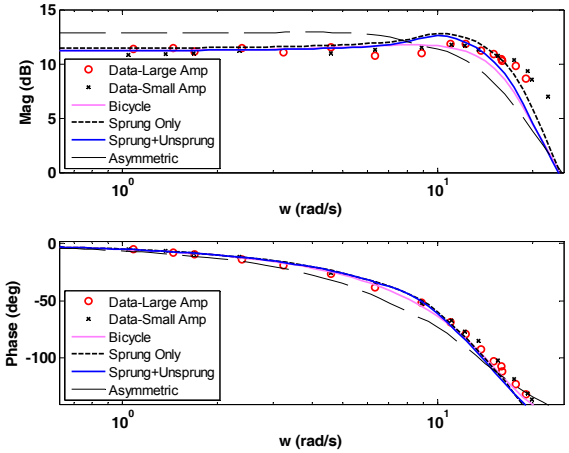

Figure 6: Frequency Resp. Steering Input to Yaw Rate

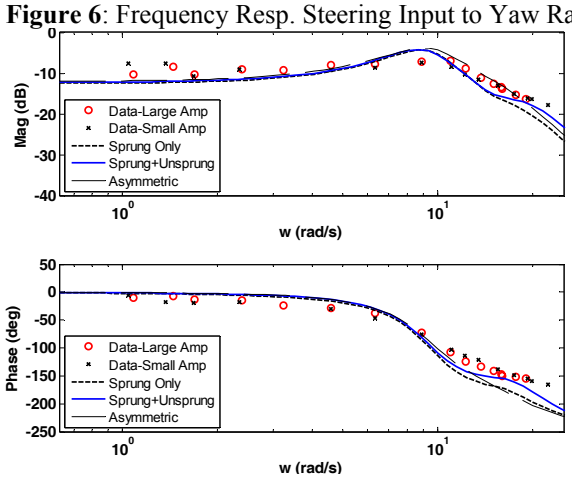

Figure 7: Frequency Resp. Steering Input to Roll Angle

Several points are evident from the above plots:

1) There is little difference between the models. Errors due to parameter-fitting seem to be larger than model-to-model differences.
2) The yaw rate and roll responses fit quite well. The lateral velocity has relatively large errors in fit, particularly around the roll dynamic frequencies.
3) The inclusion of asymmetry in the inertia appears unnecessary and perhaps detrimental to the model fit

B. Time Response Tests

In order to obtain a more intuitive understanding of the model fit obtained by the frequency response tests, time response data were also taken. Shown in Figs. 8-10 are state responses during a representative lane-change at 25 mph.

Both the frequency and time-domain responses showed that the predicted yaw response of all of the models is nearly identical.

A noticeable discontinuity is visible in the yaw rate response. After inspection of the raw yaw data, delays were observed on one-second intervals which correspond to both the SPAN system's internal Kalman filter updates and the differential corrections from the GPS base station. Investigation is ongoing to find the exact source and solution to this error.

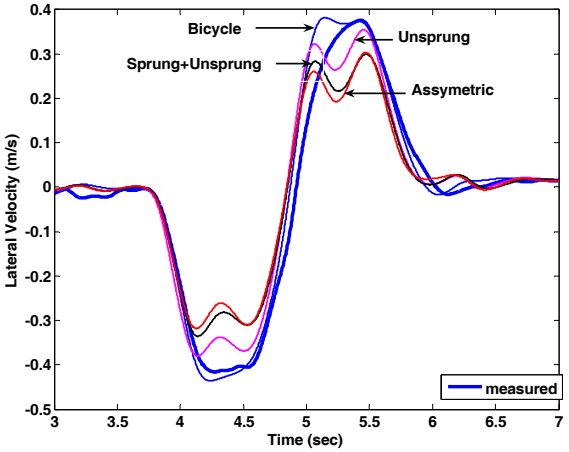

Figure 8: Lane Change Lateral Velocity Response,

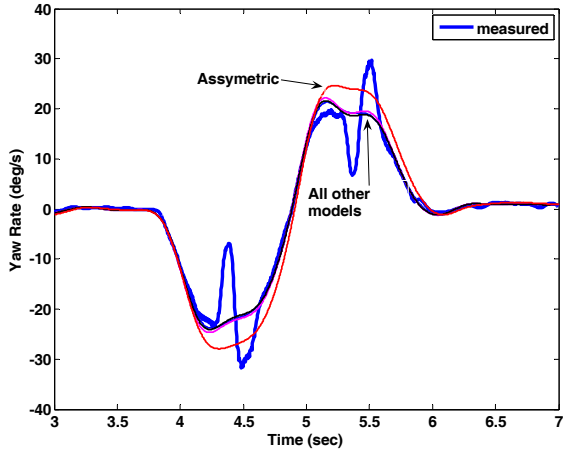

Figure 9: Lane Change Yaw Rate Response

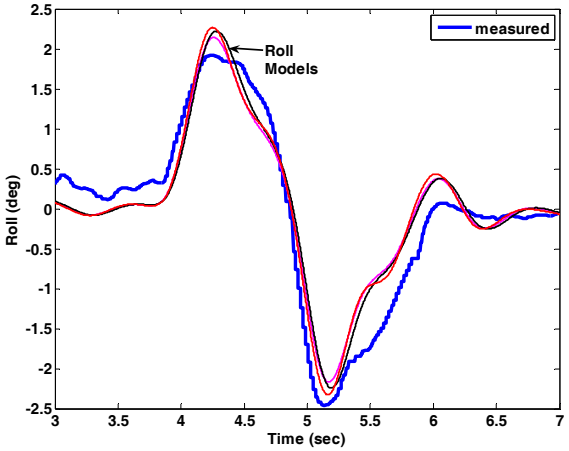

Figure 10: Lane Change Roll Response

VIII. CONCLUSIONS

An overview of ongoing work to model and validate vehicle roll dynamics was given. Several models of behavior are considered, each with different assumptions on vehicle behavior. Experimental measurements show good agreement with these simple models, but also show that model-to-model differences in vehicle behavior are not very significant. In fact, these differences appear less significant than errors observed in parameter fitting.

Further work is currently under way to better verify vehicle parameters and to obtain improved models of vehicle behavior. One evident shortcoming in the approach used thus far is the requirement that all of the models be linear. Herein lies a significant difficulty in model-based rollover prediction and model-based controller synthesis to prevent vehicle rollover: while linearity greatly simplifies controller design, the limit handling maneuvers that ultimately induce rollover nearly always involve large tire forces and tire saturation. However, prior to examining non-linear models and control schemes, it is important to fully understand and control vehicles dynamics in the linear range.

REFERENCES

[1] "Web-based Injury Statistics Query and Reporting System (WISQARS): Years of Potential Life Lost (YPLL) Reports, 1999 - 2002," Atlanta, Georgia: The Center for Disease Control (CDC), 2002.

[2] - "Leading Causes of Death Reports, 1999 - 2002,"

[3] "Traffic Safety Facts 2003 - Final Report," U.S. Department of Transportation: National Highway Traffic and Safety Board 2004.

[4] USDOT, "An Experimental Examination of Selected Maneuvers That May Induce On-Road Untripped, Light Vehicle Rollover - Phase II of NHTSA's 1997-1998 Vehicle Rollover Research Program," NHTSA report HS 808 977, July 1999.

[5] USDOT, "A Comprehensive Experimental Examination of Selected Maneuvers That May Induce On-Road, Untripped, Light Vehicle Rollover - Phase IV of NHTSA's Light Vehicle Rollover Research Program," NHTSA report HS 809 513, October 2002.

[6] J. Cameron and S. Brennan, "A Comparative, Experimental Study of Model Suitability to Describe Vehicle Rollover Dynamics for Controller Design," presented at the 2005 ASME IMECE.

[7] C. R. Carlson and J. C. Gerdes, "Optimal Rollover Prevention with Steer-by-Wire and Differential Braking," presented at 2003 ASME IMECE.

[8] H.-J. Kim and Y.-P. Park, "Investigation of robust roll motion control considering varying speed and actuator dynamics," *Mechatronics*, 2003.

[9] S. Mammar, "Speed Scheduled Vehicle Lateral Control," presented at Proceedings of the 1999 IEEE/IEEJ/JSAI International Conference on Intelligent Transportation Systems, 1999.

[10] S. Mammar, V. B. Baghdassarian, and L. Nouveliere, "Speed Scheduled Vehicle Lateral Control," presented at Proceedings of the 1999 IEEE/IEEJ/JSAI International Conference on Intelligent Transportation Systems (Cat. No.99TH8383), 1999.

[11] D. Karnopp, *Vehicle Stability*. New York: Marcel Dekker, Inc., 2004.

[12] T. Ford, J. Neumann, M. Bobye, and P. Fenton, "OEM4 Inertial: A Tightly Integrated Decentralised Inertial/GPS Navigation System," presented at Proceedings of ION GPS '01, Salt Lake City, Utah., 2001.

[13] G. J. Heydinger, R. A. Bixel, W. R. Garrott, M. Pyne, J. G. Howe, and D. A. Guenther, "Measured Vehicle Inertial Parameters - NHTSA's Data Through November 1998," *Society of Automotive Engineers*, 1999.

[14] M. Mitschke, *Dynamik der Kraftfahrzeuge*, vol. A, B, C. Berlin: Springer Verlag, 1995.

[15] T. D. Gillespie, *Fundamentals of Vehicle Dynamics*: SAE, 1992.

[16] G. J. Heydinger, W. R. Garrott, J. P. Chrstos, and D. A. Guenther, "Dynamic Effects of Tire Lag on Simulation Yaw Predictions," *Journal of Dynamic Systems, Measurement and Control,* , vol. 116, pp. 249-256, 1994.

[17] H. B. Pacejka, *Tire and Vehicle Dynamics*. Warrendale, PA: SAE Press, 2002.